DRAFT VERSION APRIL 30, 2016
Preprint typeset using LaTeX style emulateapj v. 12/16/11

COMPACT CORE GALAXIES IN THE RESOLVE SURVEY

ELAINE M. SNYDER[1], SHEILA J. KANNAPPAN[1], DARA J. NORMAN[2], MARK A. NORRIS[3], CALLIE HOOD[1], ASHLEY S. BITTNER[1], KATHLEEN D. ECKERT[1], IAN DELL'ANTONIO[4], SAMANTHA DALLAS[4], AMANDA J. MOFFETT[1,5], DAVID V. STARK[1], AND THE RESOLVE TEAM

[1]Department of Physics and Astronomy, University of North Carolina, 141 Chapman Hall CB 3255, Chapel Hill, NC 27599, USA; emsnyder@live.unc.edu
[2]National Optical Astronomical Observatory, 950 N Cherry Ave, Tucson, AZ 85719, USA
[3]Jeremiah Horrocks Institute, University of Central Lancashire, Preston, PR1 2HE, United Kingdom
[4]Department of Physics, Brown University, Box 1843, 182 Hope Street, Barus & Holley, Providence, RI 02912 and
[5]International Centre for Radio Astronomy Research (ICRAR), The University of Western Australia, 35 Stirling High- way, Crawley, WA 6009, Australia

Draft version April 30, 2016

ABSTRACT

We analyze the complete set of 96 "compact core galaxies" (CCGs) in the volume-limited RESOLVE survey to investigate their formation and evolution in relation to compact galaxies such as ultra compact dwarfs (UCDs), compact ellipticals (cEs), and dwarf ellipticals (dEs) across a broad statistical distribution of environments. To identify CCGs, we use GALFIT to perform one- and two-component Sérsic fits for all galaxies in RESOLVE with UKIDSS Y-band imaging (98% of the survey), which produces seeing-deconvolved effective radius ($R_{\rm eff}$) measurements. The one component fits are used to select candidate CCGs with $R_{\rm eff} < 1000$ pc, and we then perform new two component fits to these galaxies with the Sérsic n of the second component held fixed at 1 for an exponential disk. We finalize the CCG sample by selecting on core-only (first component) $R_{\rm eff} < 800$pc, an upper limit that encompasses all of the similarly compact stellar systems (UCDs, cEs, dEs) included in the Archive of Intermediate Mass Stellar Systems (AIMSS) catalog. We quantify the amount of light in the core and envelope of each CCG by taking the logarithm of the ratio of the light in each component. The result is a smooth continuum of CCGs that range from envelope-dominated to core+envelope to core-dominated. With GALEX NUV, SDSS *ugriz*, and 2MASS/UKIDSS $YJHK$ data, we derive colors and star formation histories and find that a significant number of CCGs live on the blue sequence and have recently formed stars. We find that CCGs naturally occur in a range of environments from isolated to cluster. We also derive velocity dispersions (σ) for 8 CCGs from Gemini IFU data and SOAR spectroscopy. Comparing to other RESOLVE galaxies and AIMSS cEs/dEs, we search for CCGs offset to higher or lower dispersion in the dispersion-stellar mass relation, which may indicate tidal stripping or dissipative formation, respectively. Initial results show 6 CCGs likely following the dissipative formation track and 2 CCGs that are slightly offset to higher σ.

Keywords: galaxies: formation, evolution — surveys

1. INTRODUCTION

The term compact stellar system (CSS) encompasses a class of galaxies that spans the radius range between globular clusters (GCs) and normal elliptical galaxies (Es). Different types of CSSs include compact elliptical galaxies (cEs; Faber 1973) and ultra compact dwarf galaxies (UCDs; Phillipps et al. 2001). There are many unanswered questions about how CSSs form and evolve through time. One fact that makes the study of these compact galaxies so intriguing is their apparent scarcity, which raises the question as to whether they are an intermediate and short-lived evolutionary phase in the life of a galaxy, or simply hard to find due to their size. Only in the last 15 years have we discovered enough (~ 40) of these objects to enable studies of their formation scenarios and evolution over cosmic time.

CSSs have radii ranging typically from $\sim$10–600 pc (e.g., Norris et al. 2014), and there are multiple ideas for how they form. The smaller of the CSSs, UCDs may simply be the high mass extension of the GC population (Drinkwater et al. 2000; Mieske et al. 2002). The is also evidence that UCDs are created via the tidal stripping of nucleated dwarf galaxies (Bekki et al. 2001; Bekki & Freeman 2003; Jennings et al. 2015; Zhang et al. 2015). Seth et al. (2014) find a supermassive black hole at the center of another UCD, providing further evidence of tidal stripping being common for UCDs. Similarly, cEs are thought to be the result of tidal stripping events, as argued for the prototypical cE, M32 (Choi et al. 2002; Graham 2002; Huxor et al. 2011). More evidence is provided by the discovery of tidal streams near cEs (Smith Castelli et al. 2008; Chilingarian et al. 2009) and one cE, studied in Kormendy et al. (1997), that is believed to host a central massive black hole. On the other hand, Wirth & Gallagher, J. S. (1984); Kormendy et al. (2009); Kormendy & Bender (2012) argue that cEs are the low mass extension to the normal E population created via dissipative formation in gas rich environments, such as mergers or in the two-phase formation process detailed in Oser et al. (2010). One of the most successful recent searches for CSSs is the AIMSS catalog (Norris et al. 2014): with many newly discovered UCDs and cEs to examine, the authors argue that both the high-mass GCs and tidal stripping scenarios are likely for UCD formation and both tidal stripping and low-mass E scenarios are likely for cE formation.

In contrast to CSSs, dwarf elliptical galaxies (dEs) and their nucleated counterparts (dE,Ns) are quite common, especially in clusters where they were first discovered. In fact, Binggeli & Cameron (1991) find that of 225 galaxies present in the center of Virgo cluster, 174 are classified as dEs or dE,Ns based on their surface brightness profiles. dEs are typically larger than CSSs with radii ranging up to $\sim$ 800 pc, whereas dE,Ns may have larger envelopes with a core radius <800 pc (e.g., Norris et al. 2014). Similar to cEs, dEs are often thought to be either tidally stripped remnants (Crnojević et al. 2014) or the low mass extension to elliptical galaxies (Kormendy & Bender 2012). They could also be the remnants of late-type disk galaxies or luminous blue compact dwarfs that have been ram-pressure stripped and often quenched as they enter the cluster environment (Lisker et al. 2013; Crawford et al. 2016). There is also some evidence that dE,Ns are the progenitors of UCDs as they fall deeper into the cluster core and are further stripped (Pfeffer & Baumgardt 2013; Zhang et al. 2015; Liu et al. 2015).

Given the similarities in formation scenarios between CSSs and dEs, we introduce the term "compact core galaxy" or "CCG" to encompass CSSs and dEs with radii up to 800 pc. The goal of this paper is to study these galaxies as a part of a continuum of compact galaxies in order to discern between formation scenarios. Clues to how CCGs form may be given by their environments, morphology i.e., one- or two-component structure, star formation histories, and kinematics. We highlight these data below.

Environments. CSSs have been found in a large range of environments thus far. UCDs were first discovered in the Fornax cluster (Hilker et al. 1999; Drinkwater et al. 2000) and have since been found in the cores of several other clusters (Price et al. 2009; Madrid et al. 2010; Jones et al. 2006; Mieske et al. 2009; Misgeld et al. 2008), in groups (Evstigneeva et al. 2007), and near field galaxies (Hau et al. 2009; Norris & Kannappan 2011). M32 was first discovered in our Local Group (Faber 1973) near M31, and more cEs have later been found in clusters (Chilingarian et al. 2007; Smith Castelli et al. 2012; Price et al. 2009) and other groups (Huxor et al. 2011; Chilingarian & Bergond 2010). As stated previously, dEs and dE,Ns are common in clusters (Smith Castelli et al. 2012; Koo et al. 1994; Guzmán et al. 1996; Crawford et al. 2016), but have also been found near groups (Crnojević et al. 2014; Penny et al. 2014). Only cEs have been found "free floating", meaning there is no host galaxy at all: Huxor et al. (2013), Paudel et al. (2014), and Chilingarian & Zolotukhin (2015) find cEs separated from other galaxies by > 1 Mpc.

Environment bears on formation scenarios in different ways. One possibility is that CSSs found in group or cluster environments may be tidally stripped remnants, whereas free floating CSSs may rather be dissipatively formed like Es. However, Chilingarian & Zolotukhin (2015) argue that these free-floating cEs could actually be tidally-stripped cores that are ejected from groups and clusters during the tidal stripping process. The recent discovery of a free-floating GC and UCD that have likely been tidally stripped in Sandoval et al. (2015) supports this idea.

Morphologies. CSSs have been found to exhibit either one component (i.e., just a core) or two component (i.e., a core plus a surrounding envelope of gas and stars) morphology. Graham (2002) have shown that M32's light profile is best fit with a core plus a surrounding exponential disk profile, which they argue points toward a tidal-stripping origin. Pfeffer & Baumgardt (2013) use N-body simulations to predict that UCDs that are tidally stripped remnants will also display multi-component surface brightness profiles due to lingering outer galaxy structures. Conversely, dissipative processes such as the two-phase formation scenario proposed by Oser et al. (2010) cause cores to form as gas rushes to the center and star formation begins. This core is then "puffed up" through time as it interacts with other galaxies. The free-floating cE discovered in Huxor et al. (2013), shown to have only a one-component light profile, may be an example of the first step in this two-phase formation. It's important to note that these effects may vary based on the degree of stripping and how much time has passed since the stripping or dissipative formation occurred.

Since dEs and dE,Ns are already divided into one and two component categories, it's easier to see the two morphologies are commonly found. Mastropietro et al. (2005) use the N-body simulations to show that as the progenitors of dEs enter clusters, their morphologies are greatly disrupted but disks may not completely destroyed by ram pressure or tidal stripping. The authors go on to argue that this excludes dEs as being the progenitors of UCDs, however, Pfeffer & Baumgardt (2013) seems to dispel this notion.

Star formation histories. Colors and star formation rates are useful since they may point to recent star formation as a part of tidal stripping or dissipative formation. The typical thought is that CSSs are "red and dead", and some studies even cut on color when selecting CSS samples. Drinkwater et al. (2000) have examined the stellar populations of CSSs and find that CSSs are usually best fit as having older stellar populations. Norris & Kannappan (2011) find a similar result with one UCD best fit using older stellar populations. Drinkwater et al. (2000) and Ferrarese et al. (2006) find that the cores of dE,Ns tend to have younger stellar populations compared to their host galaxies.

Kinematics. The last useful tool we have for discerning between formation scenarios is the galaxy's stellar velocity dispersion (σ). Bender et al. (1992) and Bekki & Freeman (2003) show that σ will remain largely unchanged when tidal stripping occurs, even though the $R_{\rm eff}$ and stellar mass will be greatly reduced. Thus, galaxies that are offset to higher σ in a Faber-Jackson (stellar mass – σ) relation (Faber & Jackson 1976) are most likely tidally stripped, while galaxies falling along the relation are most likely the low-mass extension of normal Es.

In this paper, we present a complete sample of CCGs derived from the volume-limited RESOLVE survey that have key data quantifying their morphologies, environments, star formation histories, and kinematics. We use this sample to examine the formation scenarios and evolution of CSSs and dEs/dE,Ns simultaneously as a spectrum of compact galaxies that span the gap from GCs to Es. Because we have derived a complete sample from RESOLVE, our sample contains CCGs at every evolutionary stage. This paper is organized as follows. We describe our parent sample, the RESOLVE survey, in § 2.1 and our comparison sample, the AIMSS catalog, in § 2.2. Our methods for performing seeing-deconvolved one and two component fits for the entire RESOLVE sample using GALFIT are presented in § 2.3.1. We then detail the selection of the CCG sample from the RESOLVE survey and quantify our CCG demographics in § 2.3.2. We next describe our photometric, environmental, and spectroscopic data and analysis in § 3. We present a statistical distribution of environments, star formation histories, and velocity dispersions for the complete sample in § 4. In § 5, we present a discussion of our results in the context of CCG formation and evolution. Lastly, the summary and future work are given in § 6.

2. SAMPLES

2.1. *The RESOLVE survey*

We use the RESOLVE survey (Kannappan et al. 2008, Kannappan et al., in prep) as the parent sample for our census of CCGs. RESOLVE is ideal because it is an unusually complete and volume-limited survey, which allows us to find CCGs at all evolutionary stages. RESOLVE falls within the footprint of the Sloan Digital Sky Survey (SDSS, York et al. 2000), and covers equatorial strips in both semesters: A for the northern spring sky and B for the northern fall sky, which overlaps much of Stripe-82. With $H_\circ$ = 70 km s^{-1}, RESOLVE-A spans $\sim 38,400$ Mpc^3 and occupies the region $131.25° < \mathrm{RA} < 236.25°$ and $0° < \mathrm{Dec} < 5°$, while RESOLVE-B spans $\sim 13,700$ Mpc^3 and occupies the region $330° < \mathrm{RA} < 45°$ and $-1.25° < \mathrm{Dec} < 1.255°$. Both semesters cover the redshift range 4500 km s^{-1} $<$ cz $<$ 7000 km s^{-1}.

RESOLVE's exceptional completeness is obtained by making use of multiple redshift surveys to recover galaxies that were missed in SDSS due to fiber collisions, the "shredding" of galaxies in which the pipeline breaks up a single galaxy into individual pieces, so no one piece meets the magnitude cut and the intentional exclusion of low surface brightness galaxies ($\mu_{50} < 24.5$ mag arcsec^{-2}), even if they meet the magnitude cut. We supplement the SDSS main redshift survey with additional redshifts from archival sources (the Updated Zwicky Catalog (Falco et al. 1999), HyperLeda (Paturel et al. 2003), 6dF (Jones et al. 2009), 2dF (Colless et al. 2001), GAMA (Driver et al. 2011), and ALFALFA (Haynes et al. 2011)) to achieve $\sim 12\%$ higher completeness in RESOLVE-A and $\sim 25\%$ higher completeness in RESOLVE-B.

With its improved redshift recovery, RESOLVE is complete down to absolute r-band magnitudes of -17.33 and -17.0 for the A and B semesters, respectively. To derive the stellar mass limits of RESOLVE, we use the known stellar masses and magnitudes of all RESOLVE galaxies to determine the stellar mass limit above which no more than 2% of objects have an r-band magnitude fainter than the stated magnitude completeness limit. These values are $M_\star \sim 10^{8.9}$ $M_\odot$for the A semester and $M_\star \sim 10^{8.7}$ $M_\odot$in the B semester (e.g. Figure 8 in Eckert et al. 2016). In Figure 1, we plot the stellar masses against the deconvolved, one-component, half-light radius R_{eff} (see § 2.3.1) for all of RESOLVE along with the core-only R_{eff} for the CCG sample and see that these limits allow us to reach down to CSSs with sizes and masses similar to cEs.

An important caveat to RESOLVE's completeness is that the survey is preferentially incomplete for the very objects this study is focused on, cEs. Such round objects can often be mistaken for stars in redshift surveys using tools such as the `class_star` parameter in Source Extractor (Bertin & Arnouts 1996). We are engaged in ongoing efforts to use photo-z estimates to recover some of these objects.

2.2. *The AIMSS catalog*

We use the Archive of Intermediate Mass Stellar Systems (AIMSS) catalog (Norris et al. 2014; Forbes et al. 2014; Janz et al. 2015) as a reference sample for our CCGs. AIMSS is a catalog of spectroscopically confirmed CSSs found near field galaxies and in groups and clusters, and includes both literature and newly discovered objects. Their process to find new CSSs is as follows. First, a search is conducted in the Hyperleda redshift catalog (Paturel et al. 2003) for all galaxies at distances between ~ 7 and 200 Mpc (to ensure CSSs with $R_{\mathrm{eff}} > 50$ pc will be resolved in any available HST imaging) and with $M_B < -15$. Once complete, the team then searches the Hubble Space Telescope archive for WFCP2, ACS, and WFC3 imaging within 150 kpc in projection of the selected galaxies. Next, Source Extractor is run on the HST images, and candidates are identified using a training set of previously known CSSs from the literature. Once cross-matched to ensure none are previously known and vetted by eye, spectra are obtained, redshift confirmation is performed, and velocity dispersions are extracted. AIMSS also includes literature data for other UCDs, cEs, (nucleated) dEs, dwarf spheroidals, dwarf S0s, young massive clusters, and Es. AIMSS compiles M_V, stellar mass, effective radius, and velocity dispersions for each of its objects. Thus, though not a statistically-defined sample, AIMSS provides a useful reference catalog to which we can calibrate and compare our CCGs.

2.3. *CCG sample selection*

2.3.1. *Deconvolution of RESOLVE galaxies*

We begin our analysis by deriving seeing-deconvolved R_{eff} measurements for all galaxies in the RESOLVE sample. For this task we employ GALFIT (Peng et al. 2002) to deconvolve the seeing point spread function (PSF) and to perform one and two component fits on each galaxy. Deconvolution is especially important since the smallest galaxies in RESOLVE are most effected by seeing, and accurate radii measurements are crucial for the study of these objects.

GALFIT needs the following input files to function correctly: an initial input file, an image of the galaxy, a PSF image, an image mask, and a constraint file. We obtain/construct these items as follows:

The initial input file: The initial input file gives GALFIT the files paths to the image, PSF, mask, and constraint file, and also holds the initial guesses for our fit parameters. For the one component fits, we set up our input file to have a section for measuring the level of the sky background, and another section for fitting a Sérsic profile to galaxy. The Sérsic model will find a best fit for the following parameters: central x & y position of the model, integrated magnitude, R_{eff}, Sérsic n, axial ratio (b/a), and position angle. These initial values for these parameters can just be rough guesses, but for our purposes, we use values for the magnitude, R_{eff}, b/a, and PA that are derived from RESOLVE's photometric data (see § 3.1 for more details)

Imaging data: We use publicly-available high resolution Y-band imaging from the UKIDSS Large Area Survey (Lawrence et al. 2007). This data set was chosen because it covers both RESOLVE-A and RESOLVE-B and offers $\sim 0.8''$ seeing resolution corresponding to ~ 350pc at RESOLVE distances in turn letting us span down to the sizes of cE-like galaxies. The Y band is advantageous too, since it probes the underlying stellar population and will not skew our measurements to larger radii if the galaxy is currently experiencing a starburst. We download $\sim 10' \times 10'$ images of each galaxy from the WFCAM Science Archive[1]. While GALFIT does not require images this large to operate normally, we choose this size so that there will be more stars in the field of view which is useful for constructing a PSF. There are only 25 galaxies in RESOLVE (2% of the survey) that do not have UKIDSS imaging and thus are excluded from our analysis.

[1] `was.roe.ac.uk//`

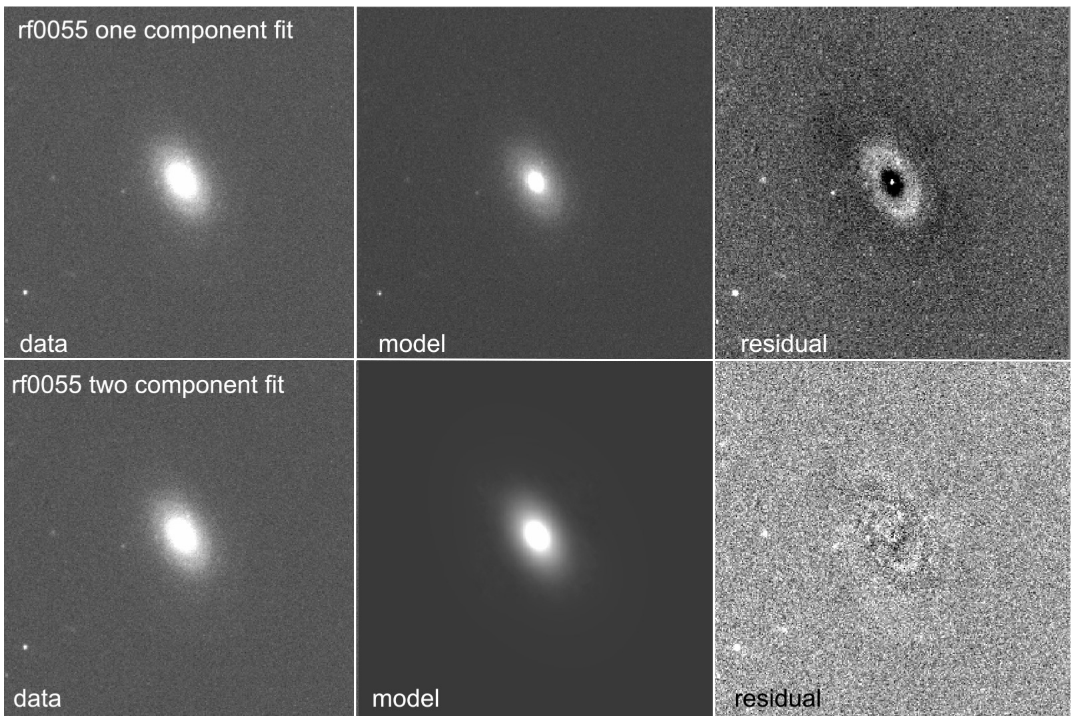

Figure 1. Shown here are the model outputs from GALFIT. The left column shows the UKIDSS Y-band image cut out around the galaxy. The middle column shows the best fit GALFIT model, and the right column shows the residuals (data-model). The top row shows the one component fit for one of the RESOLVE galaxies, rf0055. As seen in the residual image, the model is overfitting the inner bulge, and underfitting the outer envelope. The bottom row shows the two component fit for the same galaxy. We now are able to well fit both the inner bulge and the outer envelope. The residual is much cleaner, although there may be some spiral structure remaining that could require a third component to fit.

The PSF image: GALFIT uses the PSF image to deconvolve the galaxy light profile from the seeing, thereby removing the effects of atmospheric scattering of the galaxy light as the data was taken. We build our PSF image via the following steps.

1. We begin by running Source Extractor on the image to identify every object in the frame, including stars, galaxies, and even sometimes hot pixels. Source Extractor outputs a text file that has estimates of each object's flux, elongation, ellipticity, radius, and `class_star`.
2. With this information, we select stars to use for building our PSF. The limiting parameters are (1) that the flux must be between $5,000-100,000$ counts to ensure no extremely faint or saturated stars are included, (2) that the ellipticity be less than 0.2 to ensure we are selecting round objects, (3) that the effective radius of the star be greater than 1 pixel to avoid selecting hot pixels, and (4) that `class_star` is greater than 0.6 to ensure the objects we're picking are most likely stars. We also make sure the stars are not near the image edges, since there can sometimes be image artifacts there. Lastly, we make sure to not include the galaxy we are going to fit, since the cE-like galaxies can sometimes appear to be stars.
3. We next make 101×101 pixel cutouts of each object detected, with the flux peak at pixel $x = 51, y = 51$.
4. Background subtraction is then performed by taking the median of the entire cutout and then subtracting each pixel by this median value.
5. We then reject any of the cutouts that have a background median value greater than 2σ from the mean of the background median values for every cutout. This ensures we are not including any cutouts that have stars with large or bright neighboring objects. We are now left with background-subtracted cutouts of stars with no neighbors that could affect our stacking.
6. Before we can combine all the cutouts, we must normalize the flux of each central star to the same amplitude. To do this, we run each cutout through Source Extractor once more to obtain the fluxes of each central star and use these to weight the cutouts accordingly. We calculate the weight for each cutout as follows: (1) we find the central star with the highest flux of all the cutouts and then (2) divide every flux by this maximum flux. We then divide each cutout by its corresponding weight, which makes each central star have the same amplitude.
7. We then take the median of all the weighted cutouts to create a semi-complete PSF.
8. Lastly, we normalize the semi-complete PSF from Step 7 by dividing each pixel in the frame by the total flux in the image. We find the total image flux by taking the mean of each pixel and multiplying that by the number of pixels in the image (so, 101×101). This ensures that the final PSF image is normalized, i.e., the sum of the flux in each pixel of the cutout would equal one.

Our last step is to fit a 2D Gaussian to the PSF to determine a rough estimate seeing full width half max (FWHM), as a sanity check. We find that the average FWHM for all PSFs is $\sim 0.9''$, only slightly worse than the $\sim 0.8''$ seeing expected for UKIDSS imaging.

The mask image: GALFIT uses the mask image to ignore any objects neighboring our galaxy while it is completing the fit.The first step in making the mask is to create an image that has the same dimensions as our input image but with each pixel value equaling zero. We again use Source Extractor to compile a list of all the objects in the input image, and use this list to replace the pixel values at the coordinates of the located objects with one.

The constant file: The constraint file hosts the limits we are willing to accept for each of the fit parameters. The constraints for x & y position in the image, integrated magnitude, R_{eff}, Sérsic n, axial ratio (b/a), and position angle for the one component fits are listed in Table 1. We change the constraint file for the two component fits later in the analysis.

parameter	constraint
x & y position	± 5 pixels from input value
integrated magnitude	0 – 40
R_{eff}	0.2 – 750 pixels
Sérsic n	0.1 – 8
axial ratio	0 – 1
position angle	-360 – 360

Table 1
Summary of the constraints imposed on our GALFIT models for our initial one component fits for the entire RESOLVE sample.

We use all of the above to obtain a one component, seeing-deconvolved fit for every galaxy in the RESOLVE survey. We then perform the two component fits as follows. We use the output of the one component fit as the basis of the input file for the two component fit. The first two sections in the two component fit initial input file will be identical to the output of the one component fit (except that the names of the files to be output are changed). We then add a third section to include a second Sérsic fit, and change the initial guess for R_{eff} to be double that of the one component best fit. This gives GALFIT an idea to fit on both a core and envelope. The PSF, image, and mask image will all be the same as before. We add to the constraint file the same constraints as listed in Table 1, but for the third section. In other words, there will be two sets of constraints in the file now, with the first set applying to the first Sérsic fit and the second set applying the second Sérsic fit. The constraints for each parameter are the same for both sets. We do not further constrain the two component fits since we are looking for general fits to the wide variety of galaxies in RESOLVE and do not want to over constrain our fits.

For both the one and two component fits, GALFIT outputs a text file with the best fits for central x & y position of the model, integrated magnitude, R_{eff}, Sérsic n, axial ratio (b/a), and position angle and a χ^2/ν as well as a fits file that contains the data, best fit model, and residual images. See Figure 1 for example one and two component fits for a RESOLVE galaxy.

2.3.2. *Selection of CCGs*

Now that we have seeing-deconvolved R_{eff} values for the entire RESOLVE sample, we begin our search for compact core galaxies. We use the AIMSS sample to select a maximum cutoff core-only radius for CCGs at 800 pc. This upper limit ensures that we are selecting the most compact galaxies in RESOLVE, but also lets us select a range of CSSs, including cEs and dEs. RESOLVE's lower stellar mass limit of restricts us from reaching down to UCD masses.

We start our search for CCGs by using the one component fit from the above analysis and select galaxies with R_{eff} values < 1000 pc. Since we are looking for galaxies with compact cores, going up to $R_{eff} \sim 1000$ pc allows us to select objects with cores that are dominating the light and therefore may have a smaller core R_{eff} in a two component fit. We also limit the χ^2/ν to be < 1.3, since values above this represent galaxies with large residuals left over, which are normally spirals or irregulars that we would not consider a CCG. After this selection, we are left with 124 galaxies in the CCG candidate sample.

Next, we perform new two component fits using different fitting constraints: (1) the central x and y positions are taken from the one component fit and are held constant for both Sérsic components, (2) the R_{eff} of the second Sérsic fit is constrained to always be larger than that of the first Sérsic fit, and (3) the Sérsic n of the second component is held constant at 1 for an exponentially decreasing disk profile. We let the values of R_{eff}, the integrated magnitude, b/a ratio, and PA change for both fits. By doing this, we are forcing GALFIT to fit on a core (the first Sérsic fit) and disky envelope (the second Sérsic fit) for each CCG candidate.

We then examine the fits by eye and create our final CCG sample by selecting where the core $R_{eff} < 800$ pc and $\chi^2/\nu < 1.3$ to again exclude poor fits. Our sample is thus comprised of 96 CCGs in total (63 from RESOLVE-A and 33 from RESOLVE-B). This represents $\sim 6\%$ of the total RESOLVE galaxy sample. Figure 3 shows their distribution in stellar mass and decomposed R_{eff} compared to other RESOLVE galaxies and the AIMSS cEs and dEs. For the RESOLVE sample, we are plotting the one component fits, while for the CCGs, we are plotting the core R_{eff} from the fixed two component fits.

We quantify the amount of light in the core vs. the envelope by taking a ratio of the fluxes of the core and the envelope. The flux of each component is computed with $m = -2.5 \times \log(\text{flux})$, where m is the integrated magnitude output from GALFIT. For each plot in this paper, we color code the CCGs by the logarithm of the flux ratio. CCGs with more light in the envelope will have log(flux ratio) < 0, and will hereafter be called "envelope-dominated' CCGs. CCGs with more light in the core will have log(flux ratio) > 0, and will hereafter be called "core-dominated" CCGs. CCGs with log(flux ratio) ~ 0 will have both a bright core plus an extended envelope, and will be called "core+envelope" CCGs. See Figure 2 for examples of CCGs on this continuous scale. There are some cases when GALFIT cannot find a core or an envelope, and will instead fit an extremely large and faint component instead. Where this happens (5 out of 96 cases), we classify this fit as either all core/envelope depending on which component was bad (log(flux ratio) = -1 or 1). We also see in 4 out of the 96 cases that the R_{eff} values for each component will be exactly the same value to 3-4 decimal points, indicating a probable bad fit for one component. When this occurs, we classify the galaxy as being all core (log(flux ratio) = 1).

3. METHODS

3.1. *Photometry: galaxy colors, stellar and baryonic masses, and star formation rates*

The RESOLVE survey overlaps with a number of photometric surveys, including GALEX *NUV* (Morrissey et al. 2007), SDSS-DR8 *ugriz* (Aihara et al. 2011), and UKIDSS *YHK* and/or 2MASS *JHK* (Skrutskie et al. 2006). We reprocess this photometric data to improve upon the standard SDSS data pipeline, as described in detail in Eckert et al. (2015). The main differences in this processing are (1) improved sky subtraction following Blanton et al. (2011) for SDSS photometry plus custom background subtraction for UKIDSS/2MASS, (2) the definition of elliptical apertures on the sum of the higher S/N *gri* images to determine the PA and b/a ratio of the outer disk (if present), and (3) the application of the same apertures to all bands which allows us to measure magnitudes for galaxies that may not have been detected by automated survey pipelines, especially low surface brightness galaxies in 2MASS, UKIDSS, and GALEX. Then, total magnitudes are derived for each band using an exponential outer disk fit method, curve of growth method, or color correction method (e.g., Figure 2 in Eckert et al. 2015).

Stellar masses, a long-term fractional stellar mass growth rate (FSMGR), and model colors are then derived from these reprocessed *NUVugrizYJHK* magnitudes using the spectral energy distribution (SED) modeling code described in Kannappan & Gawiser (2007), Kannappan et al. (2009), and Kannappan et al. (2013). We preferentially use model grids from Kannappan et al. (2013) that combine old simple stellar populations with 2-12 Gyr age ranges and young stellar populations with either continuous star formation from 1015 Myr ago to 0-195 Myr ago, or with a simple stellar population with ages either 360, 509, 641, 806, or 1015 Myr. A stellar mass is calculated for each model, along with a likelihood. Kannappan et al. (2013) designs their model to also estimate FSMGR, which is the ratio of stellar mass created in the last Gyr to the stellar mass previously existing(i.e., an FSMGR of 1 means that the galaxy has doubled its stellar mass in the last Gyr). Likelihood weighted model colors are also output, with AB corrections for the u band and K corrections to $z = 0$.

The HI masses for RESOLVE are from the blind 21cm ALFALFA survey (Haynes et al. 2011) and from new pointed observations with the GBT and Arecibo telescopes (Stark et al., submitted). We use these masses along with the stellar masses computed in the SED models to estimate baryonic masses, defined as $M_{bary} = M_\star + 1.4M_{HI}$.

3.2. *Environment metrics*

RESOLVE is advantageous to this study because it offers excellent environment information, allowing us to search for CCGs in all environments including groups, clusters, walls, and filaments. We explore the environments of CCGs using two different metrics: the mass of their group halo and their distance to another galaxy. The group halo mass allows us to look for CCGs that are M32–Andromeda analogs where tidal stripping may be at play, or conversely look for CCGs in large groups where ram-pressure stripping could occur. The

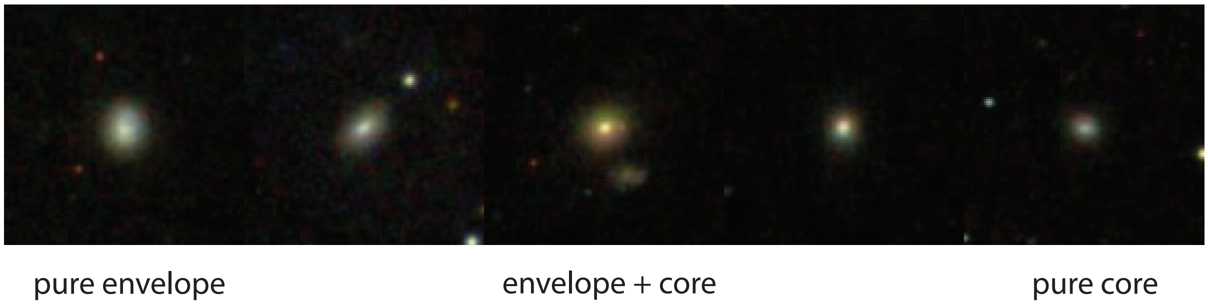

Figure 2. Five of the 96 CCGs in the final sample arranged in order from envelope-only to envelope+core to core-only. Images are taken from the SDSS-DR8 image list tool. The central image is rf0492, a CCG with possible ram pressure stripping origins (see § 4.4).

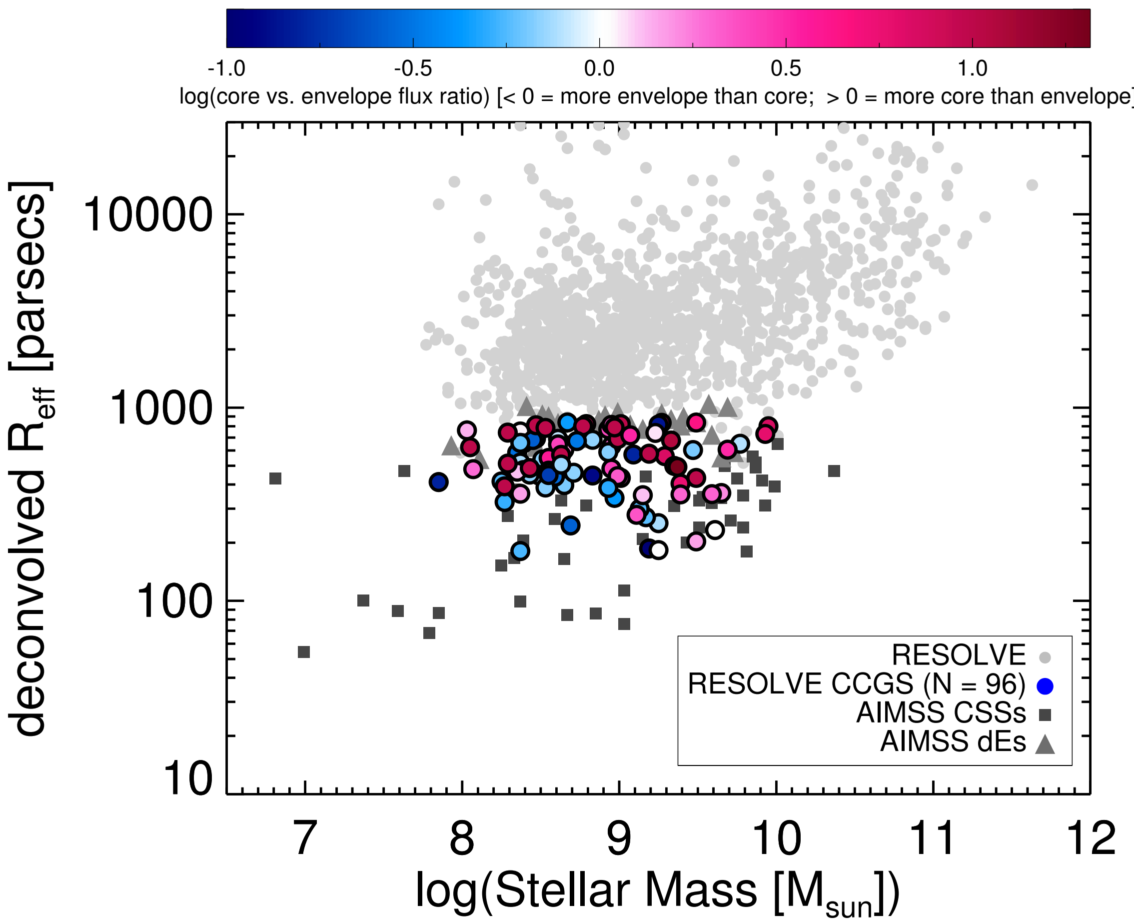

Figure 3. We plot here the deconvolved R_{eff} measurements for the entire RESOLVE sample, along with the CSSs of the AIMSS catalog. In grey are the RESOLVE (non-CCG) galaxies, which are plotted using their one component fit R_{eff}. The CCG sample is using the core R_{eff} of the two component fits, which is why they may appear separated from the full RESOLVE sample. The colors of the CCGs represent the logarithm of the flux ratio between the core and envelope. Galaxies with log(flux ratio) near 0 will have both a core and envelope, while galaxies with log(flux ratio) $\sim \pm 1$ will have more light in the core (+1) or envelope (-1).

distance to neighboring galaxies lets us examine if interaction may occur or look for analogs of the isolated galaxies found by Huxor et al. (2013) and Paudel et al. (2014).

Galaxy groups are identified using the friends-of-friends algorithm of Berlind et al. (2006), and the masses of these group halos are calculated based on the observed total r-band luminosity of galaxies in each group using abundance matching, as described in Blanton & Berlind (2007). More information on group identification can be found in Moffett et al. (2015). The nearest 2-dimensional neighbor distances are computed using the RA and Dec coordinates for each galaxy along with spherical geometry principles. Three-dimensional distances are also available with RESOLVE's redshift data, however the added errors that come with deriving peculiar velocities make these values less reliable.

3.3. *Kinematics*

3.3.1. *SOAR spectroscopy*

The RESOLVE survey gets the bulk of its spectroscopic data from the SOuthern Astrophysical Research (SOAR) Telescope, located at Cerro Tololo, Chile. We employ the Goodman Spectrograph, designed and built by UNC, along with RESOLVE's custom-built image slicer with 3 1″ slits to observe galaxies in both a broad setup and either an emission- or absorption-line kinematic setup. With this absorption-line setup, we are able to derive velocity dispersions. We use the highly-efficient 2100 l/mm VPH grating in order to cover a wavelength range 4858-5503Å, which includes stellar absorption lines such as Hβ, the magnesium triplet, and Fe5270/5335. To achieve S/N $\sim$ 25 per Å, we bin each central spectrum to $R_{\rm eff}$.

The reduction process is as follows: we use standard IRAF tasks to perform bias and overscan subtraction, trimming of the science data to remove unnecessary spatial coverage, and flat fielding. We then use LA_COSMIC (vanÂăDokkum 2001) to clean cosmic rays from each science exposure. We next complete a wavelength calibration and transformation, and then perform object tracing and extraction into a 1D spectrum using the IRAF task apall. We lastly combine the individual exposures using the IRAF task scombine.

3.3.2. *Gemini-South spectroscopy*

A subset of the faintest or smallest galaxies in RESOLVE are observed with the Gemini-South IFU for their kinematics instead of SOAR. For this absorption-line setup, we use the B1200 grating in 1-slit mode to cover a spatial region of 3″ × 5″ and the spectral range 4200-5600Å. The B1200 grating offers 0.9Å resolution when binned spectrally by 2. We calculate our exposure times such that we achieve S/N $\sim$ 25 per Å after binning by 2 in the spectral direction and summing the fibers out to $R_{\rm eff}$.

The spectral reduction proceeds as follows. Using the standard IRAF Gemini-GMOS data packages, bias and overscan subtraction, spatial trimming, flat fielding and fiber identification are performed. We next use the GMOS package gemCRspec, a wrapper for LA_COSMIC, to clean cosmic rays from each science exposure. We then correct the science frames for quantum efficiency differences between CCDs. Wavelength transformation, sky subtraction, and flux calibration are subsequently performed, and lastly, data cubes are made and summed. We then stack the individual fiber spectra out to $R_{\rm eff}$ to create a 1D spectrum for each galaxy that has S/N $\sim$ 25. More information on the data reduction for the Gemini GMOS IFU can be found in the Appendix.

3.3.3. *Velocity Dispersion Extraction*

We then derive σ from the both the SOAR and Gemini spectra using PPXF, the penalized pixel fitting code from Cappellari & Emsellem (2004). This code fits a combination of high-resolution (FWHM = 0.55 Å) ELODIE-based model spectra from Maraston & Strömbäck (2011) to the observed input spectrum, and determines a best fit solution for σ. A caveat to these fits is that they are not corrected for any stellar rotation, which will make absorption lines wider and thus skews the derived σ values toward higher values depending on the amount of rotation in each galaxy. Future work will include implementing a stellar rotation subtraction routine for these fits, but preliminary testing by binning the spectra to 1″ instead of to $R_{\rm eff}$ shows little change between the derived σ values.

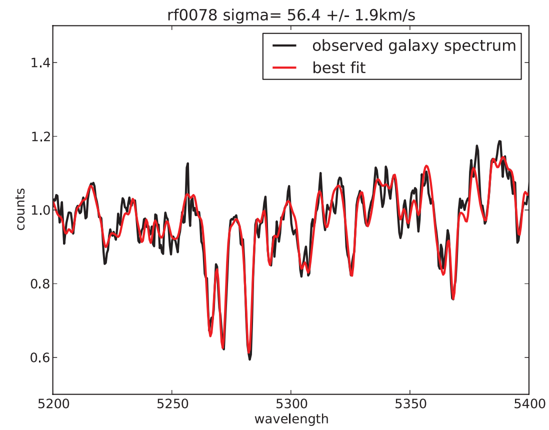

Figure 4. Plotted here in black is a summed Gemini-South IFU spectrum for the CCG rf0078. Overplotted in red is the pPXF best fit model spectrum. The spectrum is zoomed-in to show the MgB triplet fit at $\sim$ 5275 Å.

4. RESULTS

4.1. *Morphologies*

We plot in Figure 3 the deconvolved $R_{\rm eff}$ measurements for the entire RESOLVE sample, along with the CSSs of the AIMSS catalog. In grey are the RESOLVE (non-CCG) galaxies, which are plotted using their one component fit $R_{\rm eff}$. The CCG sample is also plotted with the core $R_{\rm eff}$ of the two component fits, which is why they may appear separated from the full RESOLVE sample. The symbol color for the CCGs represent the logarithm of the light ratio between the core and envelope, meaning that galaxies with log(flux ratio) near 0 will have both a core and envelope, while galaxies with log(flux ratio) $\sim \pm 1$ will have more light in the core (+1) or envelope (-1). We see in Figure 3 that both core- and envelope-dominated CCGs tend to be at the higher end of the $R_{\rm eff}$ values, while core+envelope CCGs tend to be the lower $R_{\rm eff}$ values. There also are more core-dominated CCGs at the higher $M_\star$ end while envelope-dominated CCGs tend to reside at low $M_\star$.

4.2. *Colors and Star formation rates*

We begin by examining the colors of the CCG sample. The left side of Figure 6 shows the model $u-r$ colors (as described in § 3.1) of our CCG sample plotted against $M_\star$, compared to the RESOLVE sample as a whole. An unusual finding is that many CCGs live on the blue sequence, since most CSSs are typically thought of as being "red and dead", except for those dE,Ns with bluer cores. The right side of Figure 6 shows FSMGR vs. $M_{\rm bary}$ for the same objects. As with the colors, we find that many CCGs are forming stars at a rapid rate (FSMGR $\sim$ 1 means that the galaxy has doubled its mass in the last Gyr), again an unexpected finding which could indicate that some CCGs are still in the process of forming (if dissipatively formed) or relaxing (if a tidally-stripped remnant).

Looking now at the log(flux ratio values), we see that red sequence CCGs tend to be more core-dominated, while blue sequence CCGs tend to me more envelope-dominated. There

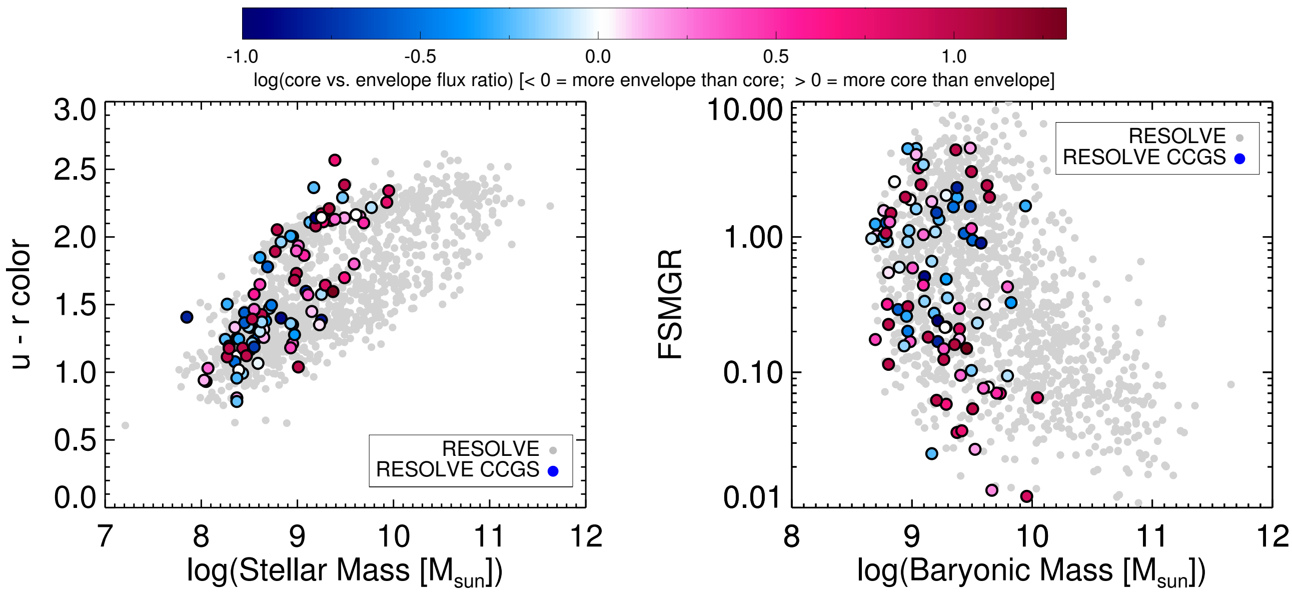

Figure 5. **(a.)** On the left we plot the $u-r$ colors against stellar mass of CCGs with the entire RESOLVE sample. **(b.)** On the right we have plotted the FSMGR against baryonic mass for both the CCGs and entire RESOLVE sample.

also tends to be more core-dominated CCGs at lower FSMGR, while envelope-dominated CCGs reside at higher FSMGR. There is considerable scatter though, making these trends harder to qualify.

4.3. *Environments*

We investigate the distribution of CCGs throughout the cosmic web, and find that CCGs span a range of different environments (see Figure 6). There are many CCGs residing in low mass groups, similar to the M32–Andromeda relationship, which suggests that tidal stripping could have occurred for those CCGs. On the opposite end, we see several CCGs in massive group halos, and that these CCGs tend to be either core- or envelope dominated. This hints towards ram pressure stripping being at play in these environments, especially for those CCGs at larger distances from other galaxies. There are also many CCGs that are > 1 Mpc away from another object in RA–Dec–redshift space, resembling the isolated cEs found by Huxor et al. (2013), Paudel et al. (2014), and Chilingarian & Zolotukhin (2015), which may point to a dissipative formation scenario since there is no nearby object to have performed the stripping.

4.4. *Kinematics*

We lastly investigate the kinematics of the CCG sample using the σs derived from SOAR and Gemini telescope data. Figure 7 plots the σ-$M_\star$ relation for the 8 CCGs with σ measurements along with the other 80+ RESOLVE galaxies with measured σs. Galaxies with σ offset to higher values point to tidal stripping occurring, since they will have more Conversely, σs that lie on the trend may point dissipative formation occurring, since these will have formed similarly to normal elliptical galaxies. Most CCGs seem to be following the dissipative merger track, and in § 5, we examine in depth the formation scenarios for each of these 8 CCGs with velocity dispersion measurements.

5. CCG FORMATION PROCESSES

We now take an in depth look at the 8 CCGs with kinematics, and assign formation scenarios based on their core $R_{\rm eff}$ morphology, star formation histories, kinematics, and environments.

5.1. *rs0345*

This mildly envelope-dominated galaxy has core $R_{\rm eff} \sim$ 450 pc. It lives firmly on the blue sequence and is forming stars quite rapidly with FSMGR ~ 1.5. Despite having a low stellar mass ($\sim 10^{8.3}$ $M_\odot$), it's baryonic (gas+stars) mass is higher than many RESOLVE galaxies, suggesting a large gas reservoir fueling star formation. The galaxy is in a moderately-sized group (halo mass $\sim 10^{11.7}$ $M_\odot$) and is within $\sim$0.15 Mpc from a companion galaxy. Taken together rs0345 may be an example of tidal stripping or dissipative formation actively occurring, which is fueling the star formation and funneling gas from the disk to build a core. Given its intermediate location between the AIMSS dEs and cEs in Figure 7 it is difficult to distinguish the formation scenario more precisely.

5.2. *rs0567, rs1186, rf0078*

Given the similarities between these three galaxies, we examine their properties together. All three are mildly core-dominated galaxies with core $R_{\rm eff}$values ranging from $\sim 200-600$ pc. They all live on the red sequence and display little star formation with FSMGR > 0.1 for all. They reside in smaller groups and have moderately close neighbors. Given their very similar σ values ranging from $\sim 50-60$ km s^{-1}, which lie along the main Faber-Jackson relation, we conclude that these three galaxies are likely dissipatively formed CCGs.

5.3. *rs1100*

Galaxy rs1100 is envelope-dominated and has one of the highest core $R_{\rm eff}$values in the same at ~ 800 pc. It is on the blue sequence and has a large FSMGR, suggesting much past star formation. It also lives in a large group with halo mass

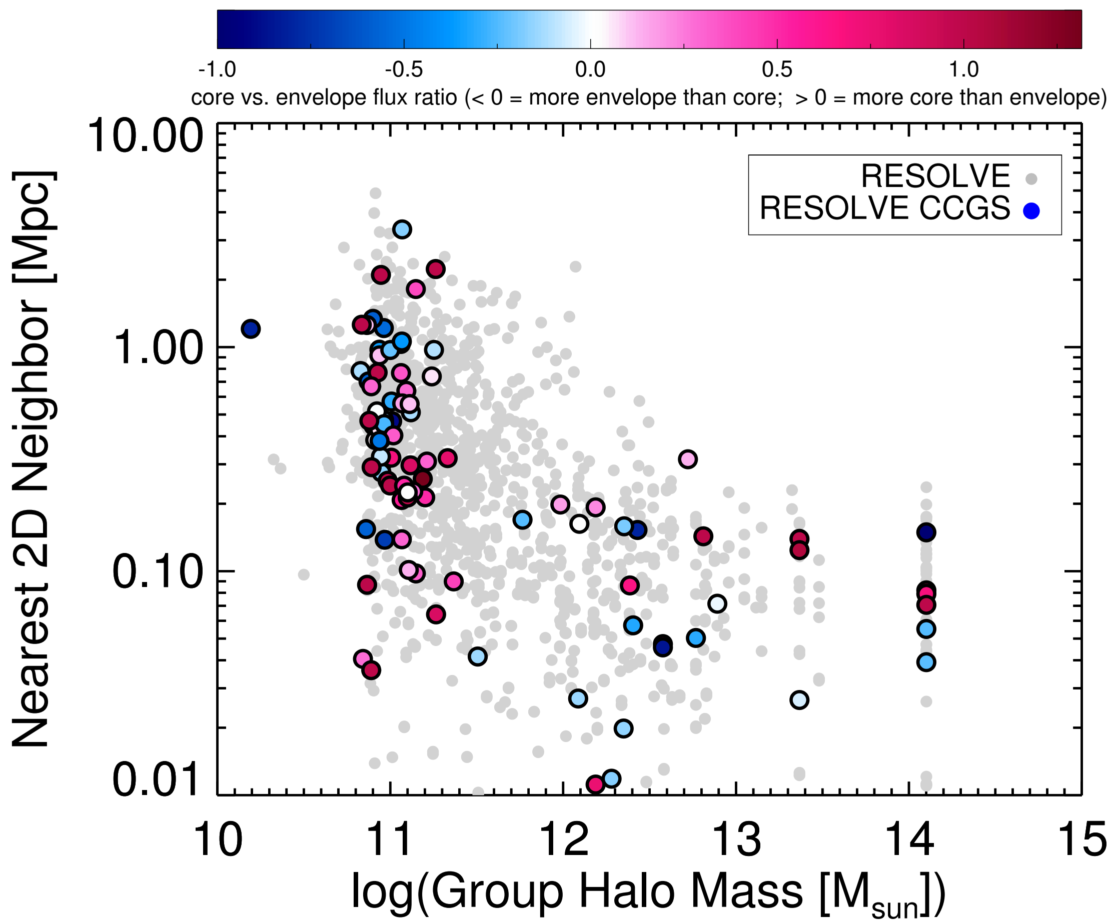

Figure 6. We plot here the group halo mass against the nearest 3D neighbor for the RESOLVE survey and CCG sample. We see that CCGs live in a variety of environments, from extremely isolated (nearest neighbor > 1 Mpc) to massive ($M_{halo} \sim 10^{13}$ $M_\odot$) groups. There is no obvious trend into whether cores+envelopes and cores/envelopes preferentially live in different environments.

$\sim 10^{12.6}$ $M_\odot$, and has a close neighbor. Its σ value places it on the dissipative formation track. We propose that rs1100 may be a galaxy in the process of being ram pressure stripped in the large group environment, or may be dissipatively forming actively.

5.4. *rf0003*

This core-dominated CCG also has a large core R_{eff} at ~ 700 pc. It lives intermediate between the blue and red sequences and has a low FSMGR, near ~ 0.10. It is also in a small group and is > 2 Mpc from another galaxy, making it perhaps a "free floating" CCG, similar to the object found in Huxor et al. (2013). Its σ places it firmly along the main Faber-Jackson relation. All together, these clues point to a dissipatively-formed CCG. However, being near the green valley may indicate that this formation occurred relatively recently.

5.5. *rf0328*

This CCG is semi-dominated by its core light, and has core $R_{eff} \sim 500$ pc. It is also in between the red and blue sequences and has a higher FSMGR at ~ 0.6, indicating considerable star formation taking place in the last Gyr. The galaxy resides in a low mass group and is ~ 0.4 Mpc from a neighbor. Its σ places it among the dissipatively formed CCGs, and like rf0003, its color and FSMGR may indicate this formation happened recently.

5.6. *rf0492*

This galaxy has core+envelope morphology and has a small core R_{eff} at ~ 200 pc. Its prominent core can be seen in the center image of Figure 2. It lives on the red sequence and has an FSMGR~ 0.08. Its nearest neighbor is 0.15 Mpc and lives in a moderately-sized group with halo mass = $10^{12.09}$ $M_\odot$. This could be an example of a CCG that was perturbed and perhaps tidal or ram pressure stripped, as it fell into this larger group, causing gas to funnel to the center to create the core we see. CCGs rs0345 and rs1100 may be the progenitors to CCGs like this one.

5.7. *CCGs without velocity dispersions*

For the other 88 CCGs without velocity dispersions, we attempt to classify their formation scenarios using the above cases as a primer. We divide the above 8 CCGs into four categories: "forming with uncertain origins" (rs0345, rs1100), "recently formed with dissipative origins likely" (rf0003, rf0328), "uncertain stripping and dissipative formation" (rf0492), and "likely dissipatively formed" (rs0567, rs1186, rf0078).

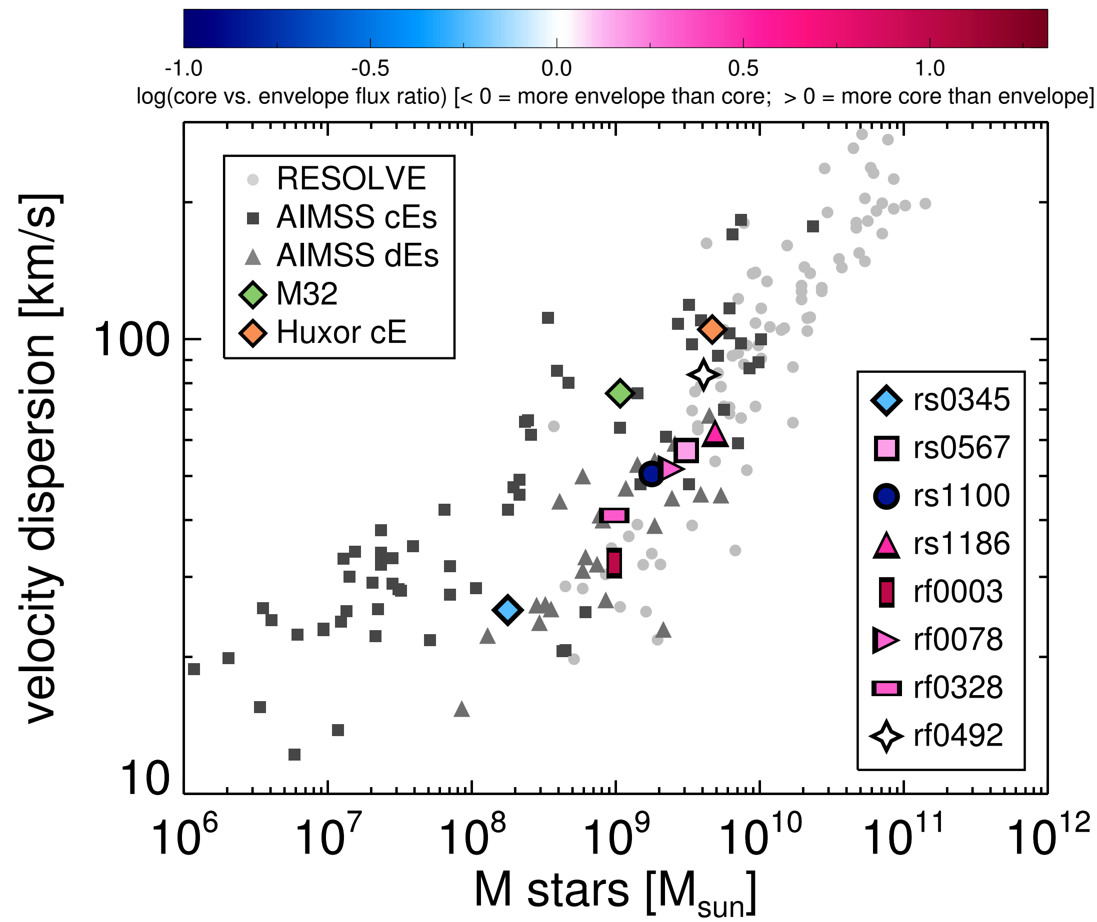

Figure 7. Plotted here is the Faber-Jackson relation (stellar mass vs. velocity dispersion) for the RESOLVE sample, CCGs, and the CSSs of the AIMSS catalog. We look for CCGs offset to higher σ for its stellar mass, which may indicate tidal stripping as a possible formation scenario. The green point is M32, the prototypical cE, that is believed to be tidally stripped (Faber 1973). In orange is the free floating cE discovered in Huxor et al. (2013) that is thought to be dissipatively formed. We see that 6 CCGs appear to be following the main Faber-Jackson trend, whereas two, rs0345 and rf0492, may be slightly offset to higher σ.

"Forming with uncertain origins" CCGs are easily characterized as having envelopes (log(flux ratio) $<$ -0.1), high FSMGR ($>$ 0.5), and living in high mass groups ($> 10^{11.5}$ $M_{\odot}$). There are 6 CCGs with these parameters ($\sim$ 1% of the sample), including the two already identified. CCGs in the "likely dissipatively formed" are also easy characterized by having cores (log(flux ratio) $>$ 0.1), low FSMGR ($>$ 0.5), and living in low mass groups ($> 10^{11.5}$ $M_{\odot}$). There are 21 CCGs with these parameters ($\sim$ 21% of the sample), again including the three already identified. This leaves 66 CCGs left to classify, but the remaining groups, "uncertain stripping and dissipative formation" and "recently formed" are more difficult to classify definitely due to their ranges of colors, morphologies, and environments. This leaves $\sim$ 69% of the CCG unclassified until more velocity information is available.

6. SUMMARY

In this paper we have examined the colors, FSMGR, environments, and kinematics of the 96 compact core galaxies (CCGs) in the RESOLVE survey. We have selected CCGs to have a seeing-deconvolved, core-only $R_{\rm eff} < 800$ pc, based on the sizes of the compact and dwarf ellipticals in the AIMSS catalog. We have quantified the amount of light in the cores and envelopes of each CCG by performing two component fits with GALFIT and taking the logarithm of the ratio of the fluxes of the two different components. CCGs with more light in the envelope have log(flux ratio) $<$ 0 and are called "envelope-dominated' CCGs. CCGs with more light in the core have log(flux ratio) $>$ 0 and are called "core-dominated" CCGs. CCGs with log(flux ratio) $\sim$ 0 have both a bright core plus an extended envelope and are called "core+envelope" CCGs. Our main results can be summarized as follows:

1. Figure 3 shows that both core- and envelope-dominated CCGs tend to be at the higher end of the $R_{\rm eff}$ values, while core+envelope CCGs tend to be the lower $R_{\rm eff}$ values. There also are more core-dominated CCGs at the higher $M_\star$ end while envelope-dominated CCGs tend to reside at low $M_\star$.

2. We find that many CCGs live on the blue sequence and are forming stars at a rapid rate (see Figure 5), which could indicate that some CCGs are still in the process of forming (if dissipatively formed) or relaxing (if a tidally-stripped remnant).

3. We find that CCGs span a range of different environments (see Figure 6). Many CCGs live in low mass groups, similar to the M32–Andromeda relationship, perhaps hinting at tidal stripping formation scenarios. Others live in massive group halos and tend to be either core- or envelope dominated CCGs, conversely hinting towards ram pressure stripping being at play. There are also many CCGs that are $>$ 1 Mpc away from another object in RA–Dec–redshift space, resembling the isolated cEs found by Huxor et al. (2013) and Paudel et al. (2014), which may point to a dissipative formation scenario.

4. Using velocity dispersions (σ) derived from the SOAR and Gemini telescopes, we look for offsets in the Faber-Jackson (σ-$M_\star$) relation that could point to tidal stripping as a possible formation scenario. In Figure 7), we find that 6 CCGs tend to follow the main Faber-Jackson trend, which is expected for galaxies formed via dissipative formation, and two CCGs that may be slightly offset to higher σ.

5. Using the 8 CCGs with velocity dispersions as a primer, we attempt to quantify the number of CCGs that are tidally stripped or dissipatively formed based on morphologies, colors, FSMGR, and environment. We estimate $\sim$6% of CCGs are actively forming (though the driver is uncertain) and $\sim$21% are likely dissipatively formed. The remaining $\sim$ 69% need more information to be classified.

Future work will include investigating the gas content and metallicities of CCGs. The amount of neutral Hydrogen gas a CCG has may be able to give us insights into its evolution over time. For example, a CCG in a galaxy cluster with little HI gas may point towards ram pressure stripping being important. Combined with CCG colors and FSMGR, the gas content may be an important tool in determining the evolution of a CCG. Janz et al. (2015) have shown that tidally-stripped CSSs are systematically offset to higher metal abundances. With the SOAR data we have in hand, we may be able to test this hypothesis for the CCG sample and use this method as another way to discern formation scenarios.

Acknowledgments. This work has been supported by funding from NSF grants AST-0955368 and OCI-1156614 and NASA grant HST-AR-12147.01-A.

REFERENCES

Aihara, H., Allende Prieto, C., An, D., et al. 2011, The Astrophysical Journal Supplement Series, 193, 29
Bekki, K., Couch, W. J., & Drinkwater, M. J. 2001, The Astrophysical Journal, 552, L105
Bekki, K., & Freeman, K. C. 2003, Monthly Notices of the Royal Astronomical Society, 346, L11
Bender, R., Burstein, D., & Faber, S. M. 1992, The Astrophysical Journal, 399, 462
Berlind, A. A., Frieman, J., Weinberg, D. H., et al. 2006, The Astrophysical Journal Supplement Series, 167, 1
Bertin, E., & Arnouts, S. 1996, Astronomy and Astrophysics Supplement Series, 117, 393
Binggeli, Â., & Cameron, Â. 1991, Astronomy and Astrophysics (ISSN 0004-6361), 252, 27
Blanton, M. R., & Berlind, A. A. 2007, The Astrophysical Journal, 664, 791
Blanton, M. R., Kazin, E., Muna, D., Weaver, B. A., & Price-Whelan, A. 2011, The Astronomical Journal, 142, 31
Cappellari, M., & Emsellem, E. 2004, Publications of the Astronomical Society of the Pacific, 116, 138
Chilingarian, I., Cayatte, V., Revaz, Y., et al. 2009, Science (New York, N.Y.), 326, 1379
Chilingarian, I., & Zolotukhin, I. 2015, Science (New York, N.Y.), 348, 418
Chilingarian, I. V., & Bergond, G. 2010, Monthly Notices of the Royal Astronomical Society: Letters, 405, L11
Chilingarian, I. V., Sil'chenko, O. K., Afanasiev, V. L., & Prugniel, P. 2007, Astronomy Letters, 33, 292
Choi, P. I., Guhathakurta, P., & Johnston, K. V. 2002, The Astronomical Journal, 124, 310
Colless, M., Dalton, G., Maddox, S., et al. 2001, Monthly Notices of the Royal Astronomical Society, 328, 1039
Crawford, S. M., Wirth, G. D., Bershady, M. A., & Randriamampandry, S. M. 2016, The Astrophysical Journal, 817, 87
Crnojević, D., Ferguson, A. M. N., Irwin, M. J., et al. 2014, Monthly Notices of the Royal Astronomical Society, 445, 3862
Drinkwater, M. J., Jones, J. B., Gregg, M. D., & Phillipps, S. 2000, Publications of the Astronomical Society of Australia, 17, 227
Driver, S. P., Hill, D. T., Kelvin, L. S., et al. 2011, Monthly Notices of the Royal Astronomical Society, 413, 971
Eckert, K. D., Kannappan, S. J., Stark, D. V., et al. 2015, The Astrophysical Journal, 810, 166
Eckert, Â., Kannappan, Â., Stark, Â., et al. 2016, eprint arXiv:1604.03957
Evstigneeva, E. A., Drinkwater, M. J., Jurek, R., et al. 2007, Monthly Notices of the Royal Astronomical Society, 378, 1036

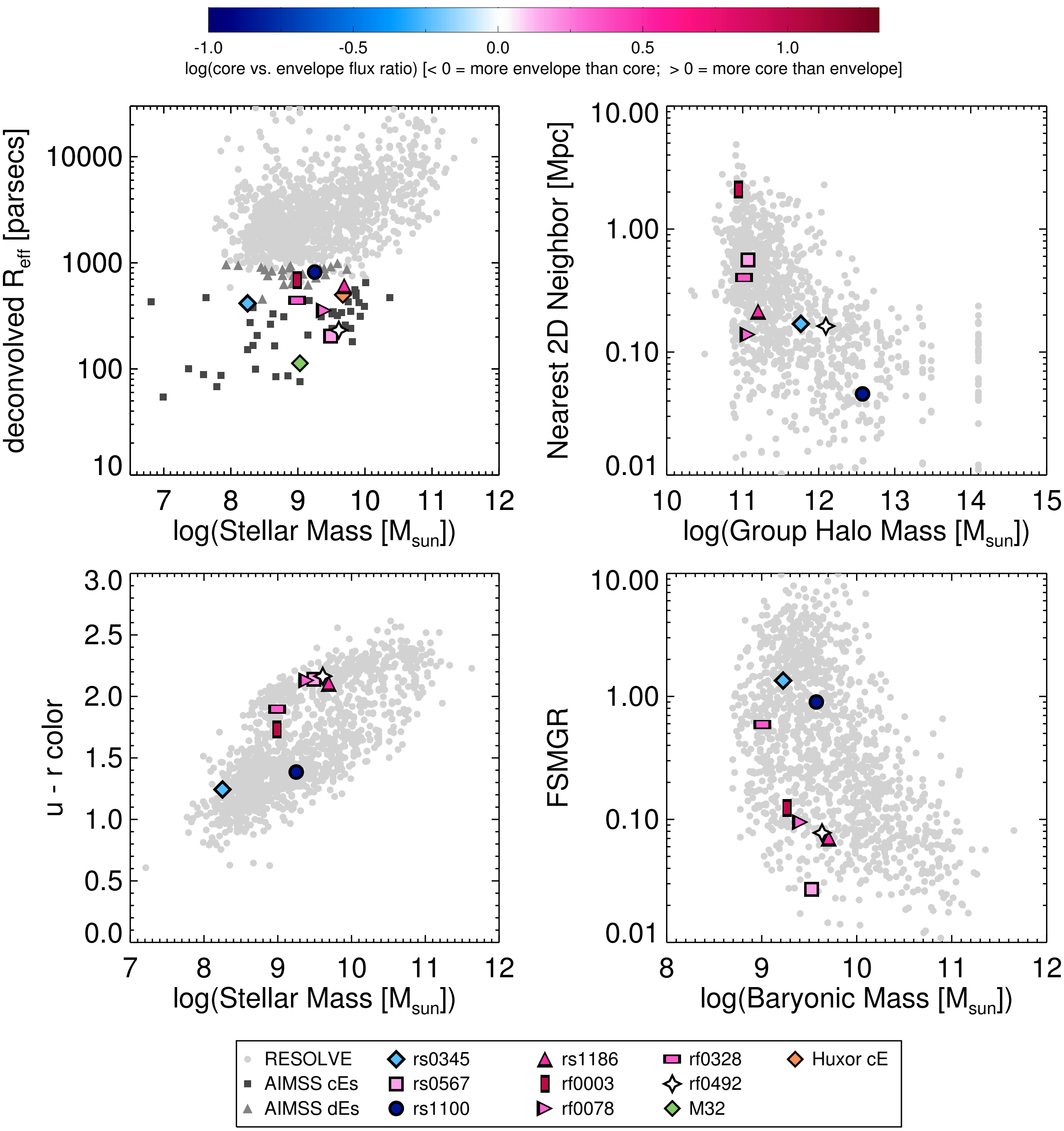

Figure 8. We show here **(a.)** deconvolved R_{eff} vs. stellar mass, **(b.)** the nearest two-dimensional neighbor vs. group halo mass, **(c.)** $u-r$ color vs. stellar mass, and **(d.)** FSMGR vs. baryonic mass for all galaxies in RESOLVE, the cEs and dEs of AIMSS, and the eight CCGs that have velocity dispersion information. This information, combined with Figure 7, help us distinguish between formation scenarios for the CCG sample.

Faber, S. M. 1973, The Astrophysical Journal, 179, 423
Faber, S. M., & Jackson, R. E. 1976, The Astrophysical Journal, 204, 668
Falco, E., Kurtz, M., Geller, M., et al. 1999, Publications of the Astronomical Society of the Pacific, 111, 438
Ferrarese, L., Côté, P., Dalla Bontà, E., et al. 2006, The Astrophysical Journal, 644, L21
Forbes, D. A., Norris, M. A., Strader, J., et al. 2014, Monthly Notices of the Royal Astronomical Society, 444, 2993
Graham, A. W. 2002, The Astrophysical Journal, 568, L13
Guzmán, R., Koo, D. C., Faber, S. M., et al. 1996, The Astrophysical Journal, 460, doi:10.1086/309966
Hau, G. K. T., Spitler, L. R., Forbes, D. A., et al. 2009, Monthly Notices of the Royal Astronomical Society: Letters, 394, L97
Haynes, M. P., Giovanelli, R., Martin, A. M., et al. 2011, The Astronomical Journal, 142, 170
Hilker, M., Infante, L., Vieira, G., Kissler-Patig, M., & Richtler, T. 1999, Astronomy and Astrophysics Supplement Series, 134, 75
Huxor, A. P., Phillipps, S., & Price, J. 2013, Monthly Notices of the Royal Astronomical Society, 430, 1956
Huxor, A. P., Phillipps, S., Price, J., & Harniman, R. 2011, Monthly Notices of the Royal Astronomical Society, 414, 3557
Janz, J., Norris, M. A., Forbes, D. A., et al. 2015, Monthly Notices of the Royal Astronomical Society, 456, 617
Jennings, Z. G., Romanowsky, A. J., Brodie, J. P., et al. 2015, The Astrophysical Journal, 812, L10
Jones, D. H., Read, M. A., Saunders, W., et al. 2009, Monthly Notices of the Royal Astronomical Society, 399, 683
Jones, J. B., Drinkwater, M. J., Jurek, R., et al. 2006, The Astronomical Journal, 131, 312
Kannappan, S. J., & Gawiser, E. 2007, The Astrophysical Journal, 657, L5
Kannappan, S. J., Guie, J. M., & Baker, A. J. 2009, The Astronomical Journal, 138, 579
Kannappan, S. J., Wei, L. H., Minchin, R., & Momjian, E. 2008, in AIP Conference Proceedings, Vol. 1035 (AIP), 163–168
Kannappan, S. J., Stark, D. V., Eckert, K. D., et al. 2013, The Astrophysical Journal, 777, 42
Koo, D. C., Bershady, M. A., Wirth, G. D., Stanford, S. A., & Majewski, S. R. 1994, The Astrophysical Journal, 427, L9
Kormendy, J., & Bender, R. 2012, The Astrophysical Journal Supplement Series, 198, 2
Kormendy, J., Fisher, D. B., Cornell, M. E., & Bender, R. 2009, The Astrophysical Journal Supplement Series, 182, 216
Kormendy, J., Bender, R., Magorrian, J., et al. 1997, The Astrophysical Journal, 482, L139
Lawrence, A., Warren, S. J., Almaini, O., et al. 2007, Monthly Notices of the Royal Astronomical Society, 379, 1599
Lisker, T., Weinmann, S. M., Janz, J., & Meyer, H. T. 2013, Monthly Notices of the Royal Astronomical Society, 432, 1162
Liu, C., Peng, E. W., Côté, P., et al. 2015, The Astrophysical Journal, 812, 34
Madrid, J. P., Graham, A. W., Harris, W. E., et al. 2010, The Astrophysical Journal, 722, 1707
Maraston, C., & Strömbäck, G. 2011, Monthly Notices of the Royal Astronomical Society, 418, 2785
Mastropietro, C., Moore, B., Mayer, L., et al. 2005, Monthly Notices of the Royal Astronomical Society, 364, 607
Mieske, S., Hilker, M., & Infante, L. 2002, Astronomy and Astrophysics, 383, 823
Mieske, S., Hilker, M., Misgeld, I., et al. 2009, Astronomy and Astrophysics, 498, 705
Misgeld, I., Mieske, S., & Hilker, M. 2008, Astronomy and Astrophysics, 486, 697
Moffett, A. J., Kannappan, S. J., Berlind, A. A., et al. 2015, The Astrophysical Journal, 812, 89
Morrissey, P., Conrow, T., Barlow, T. A., et al. 2007, The Astrophysical Journal Supplement Series, 173, 682
Norris, M. A., & Kannappan, S. J. 2011, Monthly Notices of the Royal Astronomical Society, 414, 739
Norris, M. A., Kannappan, S. J., Forbes, D. A., et al. 2014, Monthly Notices of the Royal Astronomical Society, 443, 1151
Oser, L., Ostriker, J. P., Naab, T., Johansson, P. H., & Burkert, A. 2010, The Astrophysical Journal, 725, 2312
Paturel, G., Petit, C., Prugniel, P., et al. 2003, Astronomy and Astrophysics, 412, 45
Paudel, S., Lisker, T., Hansson, K. S. A., & Huxor, A. P. 2014, Monthly Notices of the Royal Astronomical Society, 443, 446
Peng, C. Y., Ho, L. C., Impey, C. D., & Rix, H.-W. 2002, The Astronomical Journal, 124, 266
Penny, S. J., Forbes, D. A., Pimbblet, K. A., & Floyd, D. J. E. 2014, Monthly Notices of the Royal Astronomical Society, 443, 3381
Pfeffer, J., & Baumgardt, H. 2013, Monthly Notices of the Royal Astronomical Society, 433, 1997
Phillipps, S., Drinkwater, M. J., Gregg, M. D., & Jones, J. B. 2001, The Astrophysical Journal, 560, 201
Price, J., Phillipps, S., Huxor, A., et al. 2009, Monthly Notices of the Royal Astronomical Society, 397, 1816
Sandoval, M. A., Vo, R. P., Romanowsky, A. J., et al. 2015, The Astrophysical Journal, 808, L32
Seth, A. C., van den Bosch, R., Mieske, S., et al. 2014, Nature, 513, 398
Skrutskie, M. F., Cutri, R. M., Stiening, R., et al. 2006, The Astronomical Journal, 131, 1163
Smith Castelli, A. V., Cellone, S. A., Faifer, F. R., et al. 2012, Monthly Notices of the Royal Astronomical Society, 419, 2472
Smith Castelli, A. V., Faifer, F. R., Richtler, T., & Bassino, L. P. 2008, Monthly Notices of the Royal Astronomical Society, 391, 685
vanÂăDokkum, P. 2001, Publications of the Astronomical Society of the Pacific, 113, 1420
Wirth, A., & Gallagher, J. S., I. 1984, The Astrophysical Journal, 282, 85
York, D. G., Adelman, J., Anderson, Jr., J. E., et al. 2000, The Astronomical Journal, 120, 1579
Zhang, H.-X., Peng, E. W., Côté, P., et al. 2015, The Astrophysical Journal, 802, 30

APPENDIX